

Article

Phyto-Synthesis and Characterization of Silver Nanoparticles Using Box-Behnken Design and Its Anti-*Alternaria* Activity

Augustine Innalegwu Daniel ^{1,2} , Ali Al-Hashimi ¹, Marshall Keyster ³  and Ashwil Klein ^{1,*} 

¹ Plant Omics Laboratory, Department of Biotechnology, Faculty of Natural Sciences, University of the Western Cape, Robert Sobukwe Road, Bellville 7535, South Africa; 4112896@myuwc.ac.za (A.I.D.); 4178288@myuwc.ac.za (A.A.-H.)

² Department of Biochemistry, School of Life Sciences, Federal University of Technology, Minna 920101, Niger State, Nigeria

³ Environmental Biotechnology Laboratory, Department of Biotechnology, Faculty of Natural Sciences, University of the Western Cape, Robert Sobukwe Road, Bellville 7535, South Africa; mkeyster@uwc.ac.za

* Correspondence: aklein@uwc.ac.za

Abstract: *Alternaria alternata* is a global fungal pathogen that causes symptoms such as leaf blight and seed rot resulting in economically significant yield losses in different varieties of crops. Green synthesis of nanoparticles is preferred over other methods of synthesis due to their safety, eco-friendly approach, and cost-effectiveness. Phyto-synthesis of silver nanoparticles (Ag-NPs) using seed extract of *Abrus precatorious* was optimized and characterized using the Box-Behnken design (BBD). Ag-NPs with a UVmax of 409.01 nm and a crystallite and particle size of 23.75 and 34.36 nm, respectively, were synthesized. In vitro anti-*alternaria* activity of Ag-NPs showed a concentration-dependent inhibition of the mycelia with a maximum inhibition of 54.61% at 200 ppm which was significantly different ($p < 0.05$) from propiconazole (1 ppm) with 100% inhibition. A scanning electron micrograph (SEM) of mycelia treated with 200 ppm of Ag-NPs showed a shrunken and shriveled mycelia while the ultrastructure of the mycelia under a transmission electron microscope (TEM) showed the alteration of the fungus cell wall and disappearance of cellular organelles compared to the control sample, while energy dispersive x-ray spectroscopy (EDX) analysis of the mycelia showed the localization of elemental Ag (0.95%) within the cell of the fungus compared to the control. The results of this study highlighted the antifungal potential of Ag-NPs against fungicide-resistant *Alternaria alternata* to reduce the environmental impact of synthetic fungicides.

Keywords: *Alternaria alternata*; *Abrus precatorious*; box-behnken design; phyto-synthesis; silver nanoparticles



Citation: Daniel, A.I.; Al-Hashimi, A.; Keyster, M.; Klein, A. Phyto-Synthesis and Characterization of Silver Nanoparticles Using Box-Behnken Design and Its Anti-*Alternaria* Activity. *Clean Technol.* **2023**, *5*, 1381–1401. <https://doi.org/10.3390/cleantechnol5040068>

Academic Editor: Patricia Luis

Received: 18 September 2023

Revised: 3 November 2023

Accepted: 16 November 2023

Published: 30 November 2023



Copyright: © 2023 by the authors. Licensee MDPI, Basel, Switzerland. This article is an open access article distributed under the terms and conditions of the Creative Commons Attribution (CC BY) license (<https://creativecommons.org/licenses/by/4.0/>).

1. Introduction

Alternaria alternata is a global fungal pathogen that causes economically significant yield losses in different varieties of crops [1]. Preharvest leaf blight, brown leaf spot, stem canker, and postharvest fruit rot are examples of symptoms, which can vary in severity depending on the weather, host and cultivar sensitivity, and pathogen pathotype [2,3]. Additionally, the ability of *A. alternata* to produce a variety of mycotoxins like tenuazonic acid (TeA), alternariol (AOH), and alternariol monomethyl ether (AME), raises concerns about food safety. This highlights the need for effective fungal control [1].

The main strategy for decreasing the prevalence of *A. alternata* is chemical control, which uses both protective and systemic fungicides such as demethylation inhibitors (DMIs), succinate dehydrogenase inhibitors (SDHIs), and quinone outside inhibitors (QoIs) [4,5]. However, due to their widespread use and site-specific mode of action, the fungicides' therapeutic effectiveness has been compromised by the rise of resistant strains [6]. It has been reported that *A. alternata* isolates that have mutations in three of the four SDH subunits were resistant to SDHIs [7]. This was related to several mutations

in the *sdhB* subunit's position 277, the *sdhC* subunit's positions 134 and 135, and the *sdhD* subunit's positions 47, 123, or 133 in *A. alternata*'s SDH enzyme [1,8,9].

Conventional synthetic fungicides are frequently regarded as the most efficient and economical method of controlling fungal diseases [1,10]. However, because most synthetic fungicides are used often and have a site-specific mode of action, they eventually cause resistance problems and increased environmental contamination due to drug residues in water reservoirs. Since nanoparticles have the potential to improve drug distribution, delay the release of active ingredients, increase effectiveness at lower doses, and provide an environmentally friendly alternative to synthetic chemical fungicides, it has been hypothesized that they will be a key tool in resolving these issues in the future [10]. Numerous antimicrobial activities of Ag-NPs against bacteria, fungi, and viruses have been reported [11]. Furthermore, either combined with conventional fungicides or used alone, Ag-NPs have been shown to be effective against fungicide-resistant fungal pathogens [1,11,12].

Nanoparticles (NPs) have been synthesized using different techniques such as thermal, chemical, and hydrothermal methods [13]. These conventional methods for synthesizing NPs have some concerns and limitations including the use of inorganic toxic chemicals, the by-products of reducing agents, the complexity of the process, and the significant concentration of capping agents required for colloidal stability, which may cause potential environmental and biological hazards [14–16]. In addition, due to the negative effects of industrialization and urbanization on sustainable processes resulting from these methods, a new cost-effective environmentally friendly approach for synthesizing nanomaterials is at the heart of scientific research in this field [13,17]. Currently, there is a growing trend towards the use of the biological approach, known as biosynthesis or green synthesis, for the synthesis of nanoparticles, as opposed to the traditional physical and chemical methods [18]. Green synthesis of nanoparticles involves the use of microorganisms such as bacteria, fungi, algae, yeast, and plant extracts as reducing agents. This method enables the development of nanoparticles that are biocompatible and can be scaled up for large-scale production [19]. Green synthesis is a promising alternative for the synthesis of NPs because it is safe, simple, non-toxic, eco-friendly, biocompatible, and cost-effective. Furthermore, green synthesis of NPs can also enhance the properties of the produced NPs due to the specific properties of the biological substrates used and the small size and shape obtained [20].

Different factors such as pH, reaction time, type of plant extract and concentration, and temperature have been reported to play a major role in determining the size, yield, and even the nature and type of nanomaterials produced [21–23]. Therefore, to achieve a desired characteristic, a good experimental design combining an appropriate proportion of the above factors is important. A set of methods in mathematics and statistics known as the response surface methodology (RSM) employing Box-Behnken design (BBD) is a modeling technique that makes it possible to successfully complete the optimization process by identifying the effects of different components and their interactions [14]. In order to chemically optimize the conversion of AgNO₃ to Ag-NPs at a higher yield, a central composite design (CCD) under RSM was utilized [24]. Additionally, the synthesis of Ag-NPs from AgNO₃, which was biosynthesized from *Fusarium oxysporum* mycelia, was optimized using CCD under RSM [14]. Therefore, in this study, we synthesized and characterized Ag-NPs using seed extract of *Abrus precatorious* seed by employing BBD and evaluating its anti-alternaria activity. The effects of the nanoparticles on the ultrastructure and morphology, biochemical, and enzymatic activity of the fungi were also evaluated.

2. Materials and Methods

2.1. Chemicals and Reagents

Silver nitrate ($\geq 99.0\%$), sodium hydroxide ($\geq 98\%$), potato dextrose agar and potato dextrose broth, and propiconazole ($\geq 99.0\%$) were purchased from Sigma-Aldrich, Darmstadt, Germany. The Zymo Research Quick-DNA Fungal-Bacterial Miniprep kit was purchased from Zymo Research Laboratories (Irvine, CA, USA).

2.2. Isolation and Characterization of Fungal Pathogen

Alternaria alternata BBS-CT21 used in this study was isolated from the roots of diseased wheat plants collected in Cape Farms, South Africa (33°48'26.6" S 18°33'45.9" E) in 2022. Pure cultures of the fungal strain were maintained on potato dextrose agar (PDA) (Sigma-Aldrich, Germany) at 28 °C for 7 days and stored at 4 °C until further use. The genomic DNA was extracted using the Zymo Research Quick-DNA Fungal-Bacterial Miniprep kit (Research Laboratories, Irvine, CA, USA). The identification and amplification of the nuclear ribosomal internal transcribed spacer region (ITS1/ITS4) loci was carried out using the Polymerase Chain Reaction (PCR) method reported by Castaldi et al. [25]. The acquired sequence data was edited and aligned using the Cluster W multiple sequence alignment tool. The sequence was then subjected to a homology search against sequences archived in GenBank (<http://blast.ncbi.nlm.nih.gov>, accessed on 13 June 2023) to identify the fungal with the highest percentage similarity. The strain's sequence was recorded in GenBank under the name *Alternaria alternata* BBS-CT 21, with the corresponding accession number: OR235126.

2.3. Preparation of Plant Extract

Abrus precatorious seeds were obtained from Kure Ultra-Modern Market in Minna, Niger State, Nigeria. The seed was pulverized into powder using mortar and pestle and further blended into fine powder using a kitchen-type blender. Approximately 20 g of the powdered material was extracted with 400 mL of distilled water on a magnetic stirrer at 45 °C for 30 min. The extract was filtered with muslin cloth and centrifuged at a speed of 9000 × g rpm for 10 min to obtain a clear filtrate. The filtrate was stored in the refrigerator at 4 °C for future usage.

2.4. Phyto-Synthesis of Silver Nanoparticles

The phyto-synthesis of silver nanoparticles (Ag-NPs) was carried out via the green route as described by Chi et al. [26] with slight modifications. A total of 20 mL of plant extract was mixed with 100 mL of silver nitrate solution (0.2 mM) in a 1:5 ratio. The pH of the reaction medium was adjusted using 0.2 M NaOH and the mixture was stirred continuously for 2 h at 60 °C in the dark. A color change was observed after the incubation period which was an initial validation of the synthesis of Ag-NPs. The mixture was centrifuged at 9000 × g rpm for 10 min and washed continuously using deionized distilled water to collect the synthesized nanoparticles. The nanoparticles were dried in a hot air oven at 80 °C for 3 h and used for downstream analysis.

Characterization of Silver Nanoparticles

A FLUOstar Omega UV-visible spectrophotometer (BMG LABTECH GmbH, Ortenberg, Germany), X-ray Diffraction (XRD) (Bruker d8, Karlsruhe, Germany), Scanning Electron Microscopy (SEM) (Hitachi X650, Tokyo, Japan), Transmission Electron Microscopy (TEM) (Hitachi H800, Tokyo, Japan), and Energy-dispersive X-ray Spectroscopy (EDX) (Hitachi HT7800, Tokyo, Japan) were used for the characterization of Ag-NPs.

2.5. Design of Experiment

The experimental design statistical analysis was carried out using Design expert software coupled with Response surface methodology (RSM) and Box-Behnken design (BBD). In this study, a three-level, four-factor Box-Behnken design was used. The independent variables were pH, reaction time (minutes), reaction temperature (°C), and AgNO₃ concentration (mM) with their coded values −1 (minimum), 0 (center point), and +1 (maximal) (Table 1). The BBD consisted of 29 runs with 5 center points. The two dependent variables were nanoparticle size (nm) and yield (%). The nonlinear quadratic model equation shown below was used to calculate the expected Y response:

$$Y = \alpha_0 + \alpha_1 A + \alpha_2 B + \alpha_3 C + \alpha_1 \alpha_1 A^2 + \alpha_2 \alpha_2 B^2 + \alpha_3 \alpha_3 C^2 + \alpha_1 \alpha_2 AB + \alpha_1 \alpha_3 AC + \alpha_2 \alpha_3 BC \quad (1)$$

where Y was the dependent variables (calculated responses), α_0 was the intercept, α_1 , α_2 , and α_3 , were the coefficients in linear form, the interception was $\alpha_1\alpha_1$, $\alpha_2\alpha_2$, $\alpha_3\alpha_3$, and the quadratic coefficients were $\alpha_1\alpha_2$, $\alpha_1\alpha_3$ and $\alpha_2\alpha_3$ [14].

Table 1. Minimum and maximum experimental values of Box-Behnken Design for the synthesis and yield of Ag-NPs.

Factors	−1	0	1
pH	3	7.5	12
Temperature (°C)	30	60	90
Reaction time (mins)	30	75	120
Concentration (mM)	1	3	5

2.6. Anti-*Alternaria* Activity of Ag-NPs

The modified poisoned food technique, as reported by Bashir et al. [27], was used to test for the antifungal activity of Ag nanoparticles. A solution of Ag nanoparticles (2 mL) of varied concentrations (50, 100, and 200 ppm) was introduced into a 20 mm Petri dish and mixed with 18 mL of sterile PDA. The Petri dish was rocked gently to avoid air bubble formation. The plates were allowed to stand for 45 min for the media to solidify at room temperature (25 ± 2 °C). A sterile cork-borer (4 mm) was used to aseptically transfer agar plugs of 7-day-old *A. alternata* mycelia to the center of the petri plates. The same approach was used to inoculate the positive control plates (1 ppm propiconazole) and the negative control plates (no nanoparticles). The experiment was carried out in triplicates, and the plates were incubated at 27 °C. Fungal mycelia diameter measurement was recorded every day for seven consecutive days using the formula described by Philippe et al. [28] and the percentage inhibition of *A. alternata* mycelia was calculated on the seventh day:

$$\% \text{inhibition of mycelia growth} = \frac{D1 - D2}{D1} \times 100 \quad (2)$$

where D1 was the average diameter of mycelial growth in the negative control plate and D2 was the average diameter of mycelial growth in the experimental plates.

2.7. Effect of Ag-NPs on Mycelial Morphology and Ultrastructure of *A. alternata*

The effect of Ag-NPs on the morphological and ultrastructural changes of *A. alternata* was investigated using HRSEM and HRTEM as reported by Li et al. [29]. Agar plugs of *A. alternata* were sub-cultured for 7 days at 27 °C on a PDA plate containing 200 ppm of the nanoparticles. A control plate that contains no nanoparticle was used as the control. On the 7th day, mycelial fragments (about $\sim 5 \times \sim 5$ mm) from the edges of actively growing regions were collected and preserved in 2.5% glutaraldehyde for 12 h at 4 °C. The samples were taken out and washed twice, once in distilled water and twice in 10 mM PBS (pH 7.2). This was followed by a series of dehydration in ethanol of different concentrations (50, 70, 90, and 100%, v/v) for 10 min at each step prior to HRSEM analysis. For HRSEM analysis, samples were mounted on carbon support on an aluminum stub after drying to a critical drying point and then coated in gold-palladium to be observed under HRSEM.

For HRTEM analysis, mycelia samples were postfixed for 30 min with 1% osmium tetroxide in PBS (pH 7.4) overnight. The following day, the mycelia were rinsed twice in PBS (pH 7.4) for 5 min and rinsed twice in distilled water for 5 min prior to the analysis. The samples were dehydrated twice in absolute acetone for 10 min each, and once in a series of different concentrations of ethanol (50, 70, 90, 95, and 100%, v/v) for 5 min. The samples were left in 50/50 Spurr's resin and acetone overnight for embedment and the samples were taken out and placed in 75/25 resin: acetone for another 8 h before placing them in 100% resin overnight. The samples were taken out and embedded in epoxy resin for 24 h at 60 °C. Finally, the embedded samples were sliced with ultramicrotome and stained with uranyl acetate before viewing under the microscope.

2.8. Biochemical and Enzymatic Analysis of *A. alternata* Treated with Ag Nanoparticles

For the biochemical analysis, *A. alternata* was grown in potato dextrose broth (PDB) containing 200 ppm of Ag-NPs respectively for 10 days. The fungal biomass or filtrate was used for the analysis as per requirement for each assay.

2.8.1. Quantification of Extracellular and Intracellular Polysaccharides

A culture of *A. alternata* in a 200 mL potato dextrose broth (PDB) containing 200 × g ppm Ag-NPs was centrifuged, and the supernatant was used for the measurement of extracellular polysaccharides. Proteins in the supernatant were precipitated with 20 mL of 20% trichloroacetic acid (TCA). An aliquot (1 mL) of the protein-free supernatant was used to quantify extracellular polysaccharides using the Anthrone method by measuring absorbance at 620 nm.

For intracellular polysaccharides, 5 mg of *A. alternata* biomass from each treatment was ground in 10 mL of phosphate buffer (pH 6.5) under liquid nitrogen. The mixture was centrifuged at 4 °C for 20 min at 13,000 × g rpm to collect the supernatant. Approximately 20 mL of 10% TCA was added to the supernatant to precipitate proteins and 1 mL of the supernatant (free of proteins) was used to quantify intracellular polysaccharides using the Anthrone method by measuring the absorbance at 620 nm [30]. The extracellular and intracellular polysaccharide contents were calculated using the glucose standard curve (0.1–1 mg/mL).

2.8.2. Estimation of Chitin Content

A two-phase extraction procedure was used to estimate chitin using a 10-day-old *A. alternata* biomass grown in PDB containing 200 ppm of Ag-NPs. The biomass was dried in a hot air oven at 40 °C for 8–10 h. Exactly 0.5 g of the dried biomass was ground in 15 mL of 1 M NaOH and incubated for 2 h at 40 °C in a water bath. The mixture was centrifuged, and the supernatant was discarded, rinsed with distilled water, and centrifuged to collect the biomass. Potassium permanganate (5 mL, 10 g/L) was added to the biomass and incubated for 1 h at room temperature. The mixture was centrifuged, and 5 mL of oxalic acid (10 g/L) was added to decolorize the fungal biomass. Finally, the mixture was centrifuged and the biomass which contained the chitin was dried and weighed [31].

2.8.3. Cellulase Activity

A modified Mendel's growing medium was used to quantify *A. alternata* cellulase activity in response to Ag-NPs. The growth medium contained peptone (0.1%), urea (0.03%), MnSO₄·7H₂O (0.0016%), ZnSO₄·7H₂O (0.0014%), (NH₄)₂SO₄ (0.14%), MgSO₄·7H₂O (0.03%), FeSO₄·7H₂O (0.05%), CaCl₂ (0.01%), CoCl₂·6H₂O (0.0029%), KH₂PO₄ (0.2%), and cellulose (1%). Exactly 200 mL of the growth medium was autoclaved and cooled before the agar plug from a pure *A. alternata* PDA plate was aseptically transferred to the flask and incubated at 28 °C with moderate agitation (180 rpm) for 10 days. Following incubation, the cultures in the flask were centrifuged for 10 min at 4 °C, 9000 × g rpm, and the supernatant was used as crude enzyme to assay for endoglucanase (carboxymethylcellulase activity) and exoglucanase activity [32].

Endoglucanase activity was determined by incubating 1 mL of 1% (*w/v*) carboxymethylcellulase (CMC) in 0.1 M sodium acetate buffer (pH 5) for 30 min at 50 °C with 1 mL of the crude enzyme. The reduced sugar content was measured using the di-nitrosalicylic acid (DNS) method described previously by Ang et al. [33]. Exoglucanase activity was measured by incubating 1 mL of crude enzyme in 0.1 M citrate phosphate buffer (pH 4.8) with 1 mL of 0.5% cellulose for 30 min at 50 °C and the reducing sugar content was measured using the DNS method previously described by Ang et al. [33] while Cellulase activity was estimated using the method described by Dhiman et al. [34].

2.8.4. Lipase Activity

To quantify the lipase activity of *A. alternata*, the growth medium was made of the following: glucose (0.1%), olive oil (3%), NH₄Cl (0.5%), yeast extract (0.36%), H₃PO₄ (0.1%), MgCl₂ (0.01%), CaCl₂ (0.04%), and supplemented with 200 ppm of Ag-NPs. A 10-day-old agar plug of a growing mycelium from a PDA plate was inoculated into the medium and incubated for 10 days at 28 °C and 180 rpm. On the 10th day, the culture was filtered using Whatman filter paper, and the supernatant was used for the analysis of extracellular lipase activity. For intracellular lipase activity, fungal biomass was ground with 10 mL of phosphate buffer (pH 7) under liquid nitrogen and centrifuged at 13,000 × g rpm for 20 min at 4 °C to separate the supernatant which was used for the intracellular lipase activity. The reaction mixture for lipase activity (extracellular and intracellular lipase) was comprised of 1 mL of the supernatant, 10 mL of a 10% solution of olive oil in 10% gum acacia, 2 mL of a 0.6% solution of CaCl₂, and 5 mL of a 1 M phosphate buffer with a pH of 7. The mixture was incubated for one hour and agitated at 150 rpm. Following the incubation period, 20 mL of alcohol and acetone (1:1) was added into the flask to terminate the reaction. The liberated fatty acid was titrated against 0.1 N NaOH to a faint pink color using a phenolphthalein indicator [35,36].

2.9. Data Analysis

Statistical analysis was performed using GraphPad Prism version 8.0.1 and SPSS version 26. Data were expressed as the mean ± standard error of the mean (SEM) of triplicate determinations. Significant differences were analyzed using one-way analysis of variance (ANOVA). Values were considered significant at $p < 0.05$ were considered significant.

3. Results

3.1. Phyto-Synthesis and Characterization of Ag-NPs

Silver nanoparticles were synthesized using seed extract of *Abrus precatorious*. The UV-visible result (Figure 1a) showed a UVmax absorbance of 409.01 nm. Scanning electron microscope results showed face-centered cubic Ag-NPs (Figure 1b) while the transmission electron microscope showed monodispersed nanomaterials (Figure 1c) with a particle size of 34.36 ± 10.88 nm (Figure 1d). XRD results showed the appearance of peaks at 2θ values of 32.37° , 37.62° , 54.57° , 64.73° , 67.97° , and 80.38° corresponding to a diffraction plane of (200), (111), (311), (220), (400) and (222) which matched the JCP2 file number, 04-0783 (Figure 1d). The average crystallite size of Ag-NPs was estimated using the Debye Scherrer formula and was found to be ~23.75 nm. The elemental composition of the nanoparticles showed the presence of Ag and O as the most abundant element with an atomic weight of 76.49 and 22.73, respectively (Figure 1e).

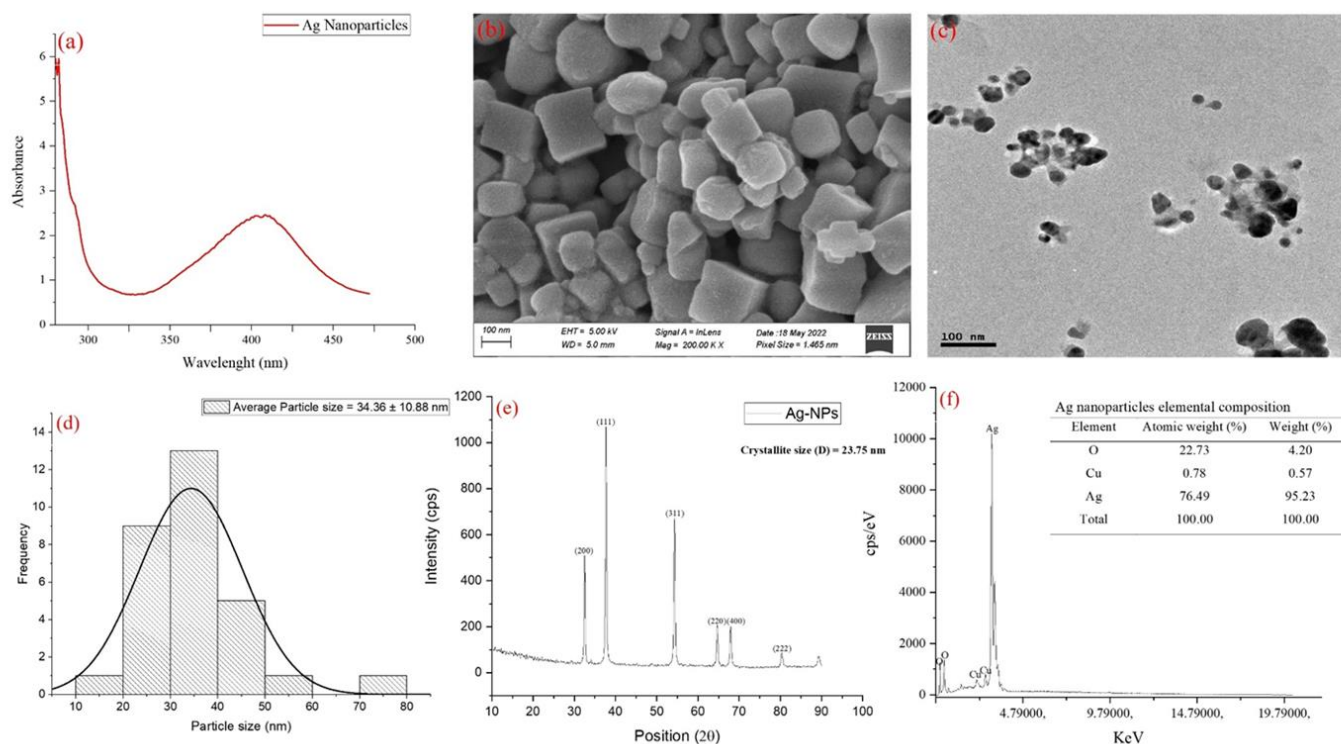


Figure 1. (a) UV-vis absorption (b) SEM image (c) TEM image (d) particle size distribution (e) XRD plot and (f) EDX plot of phyto-synthesized Ag-NPs.

3.2. Optimization Analysis of Phyto-Synthesized Ag-Nps

The actual and predicted values of the four different parameters and their corresponding responses are shown in Table S1 of Supplementary File. The smallest particle size and yield of 20.36 nm and 42.33%, respectively, were synthesized at pH 12 and a temperature of 30 °C for 75 min using 3 mM of AgNO₃ solution as the optimum conditions. Table 2 shows the analysis of variance for the response surface quadratic model for the particle size of Ag-NPs. The results showed that the model and the effect of the optimization parameters (pH, reaction time, and concentration) on the nanoparticle size were all significant ($p < 0.0001$). The effect of the optimization parameters on the yield of the nanoparticles showed a statistically significant difference ($p < 0.0001$) except for reaction time (Table 3). The predicted coded equations for nanoparticle size (nm) and the yield (%) were also given with a different combination of the optimization parameters to achieve the desired response (Equations (1) and (2)).

The 3D and 2D plots showed different combinations of the optimization parameters and the optimum values for each of the combinations to obtain a desired response of particle size and yield (Figures 2 and 3). The particle size distributions, which provide a summary of the particle size distribution, showed that 5 combinations from the optimization analysis fell within a particle size of <60 nm and 18 combinations were within 62–90 nm while 6 combinations had a particle size >90 nm (Table S1).

Table 2. Analysis of variance table for the response surface quadratic model of particle size of Ag-NPs.

Source	Sum of Squares	df	Mean Square	F-Value	p-Value
Model	16,627.92	14	1187.71	492.56	<0.0001
A-pH	6228.05	1	6228.05	2582.86	<0.0001
B-Temperature	6.31	1	6.31	2.62	0.1281
C-Reaction time	569.67	1	569.67	236.25	<0.0001
D-Concentration	3.14	1	3.14	1.30	0.2728
AB	4290.91	1	4290.91	1779.50	<0.0001
AC	101.20	1	101.20	41.97	<0.0001
AD	1273.42	1	1273.42	528.10	<0.0001
BC	103.23	1	103.23	42.81	<0.0001
BD	3980.98	1	3980.98	1650.96	<0.0001
CD	60.37	1	60.37	25.04	0.0002
A ²	9.82	1	9.82	4.07	0.0632
B ²	0.7074	1	0.7074	0.2934	0.5966
C ²	0.0685	1	0.0685	0.0284	0.8686
D ²	0.0316	1	0.0316	0.0131	0.9105
Residual	33.76	14	2.41		
Lack of Fit	30.36	10	3.04	3.58	0.1155
Pure Error	3.40	4	0.8492		
Cor Total	16,661.68	28			

R² = 0.9980, Adjusted R² = 0.9959, Predicted R² = 0.9892, Adequate precision = 99.4529.

Table 3. Analysis of variance table for response surface quadratic model for the yield of Ag-NPs.

Source	Sum of Squares	df	Mean Square	F-Value	p-Value
Model	4052.17	14	289.44	19.80	<0.0001
A-pH	499.62	1	499.62	34.18	<0.0001
B-Temperature	738.21	1	738.21	50.50	<0.0001
C-Reaction time	52.75	1	52.75	3.61	0.0783
D-Concentration	164.80	1	164.80	11.27	0.0047
AB	44.22	1	44.22	3.03	0.1039
AC	127.24	1	127.24	8.70	0.0105
AD	0.0210	1	0.0210	0.0014	0.9703
BC	132.02	1	132.02	9.03	0.0095
BD	97.61	1	97.61	6.68	0.0216
CD	222.90	1	222.90	15.25	0.0016
A ²	954.22	1	954.22	65.28	<0.0001
B ²	1354.88	1	1354.88	92.69	<0.0001
C ²	140.86	1	140.86	9.64	0.0078
D ²	240.68	1	240.68	16.46	0.0012
Residual	204.65	14	14.62		
Lack of Fit	204.03	10	20.40	131.74	0.0001
Pure Error	0.6195	4	0.1549		
Cor Total	4256.83	28			

R² = 0.9519, Adjusted R² = 0.9038, Predicted R² = 0.7237, Adequate precision = 16.9902.

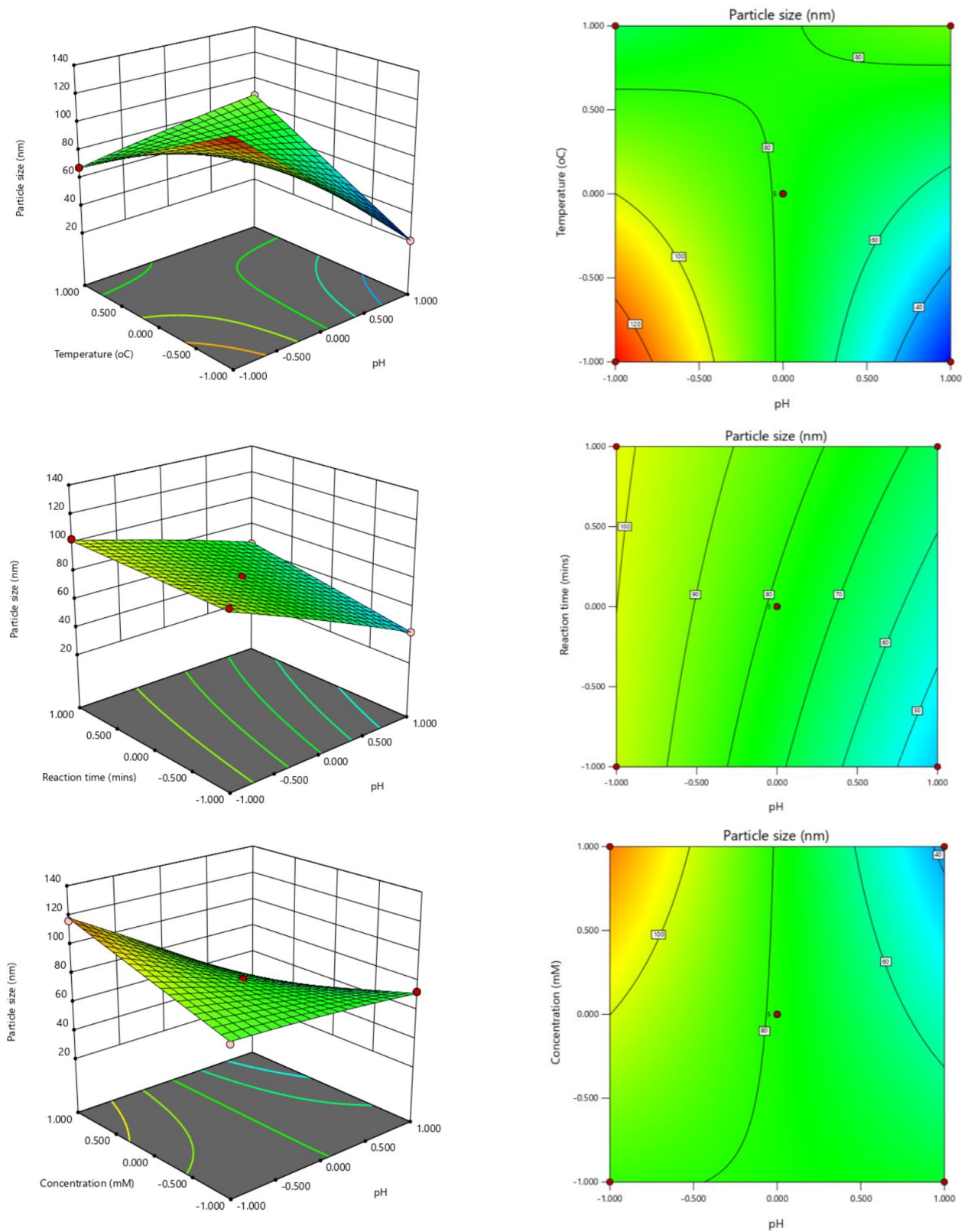


Figure 2. Cont.

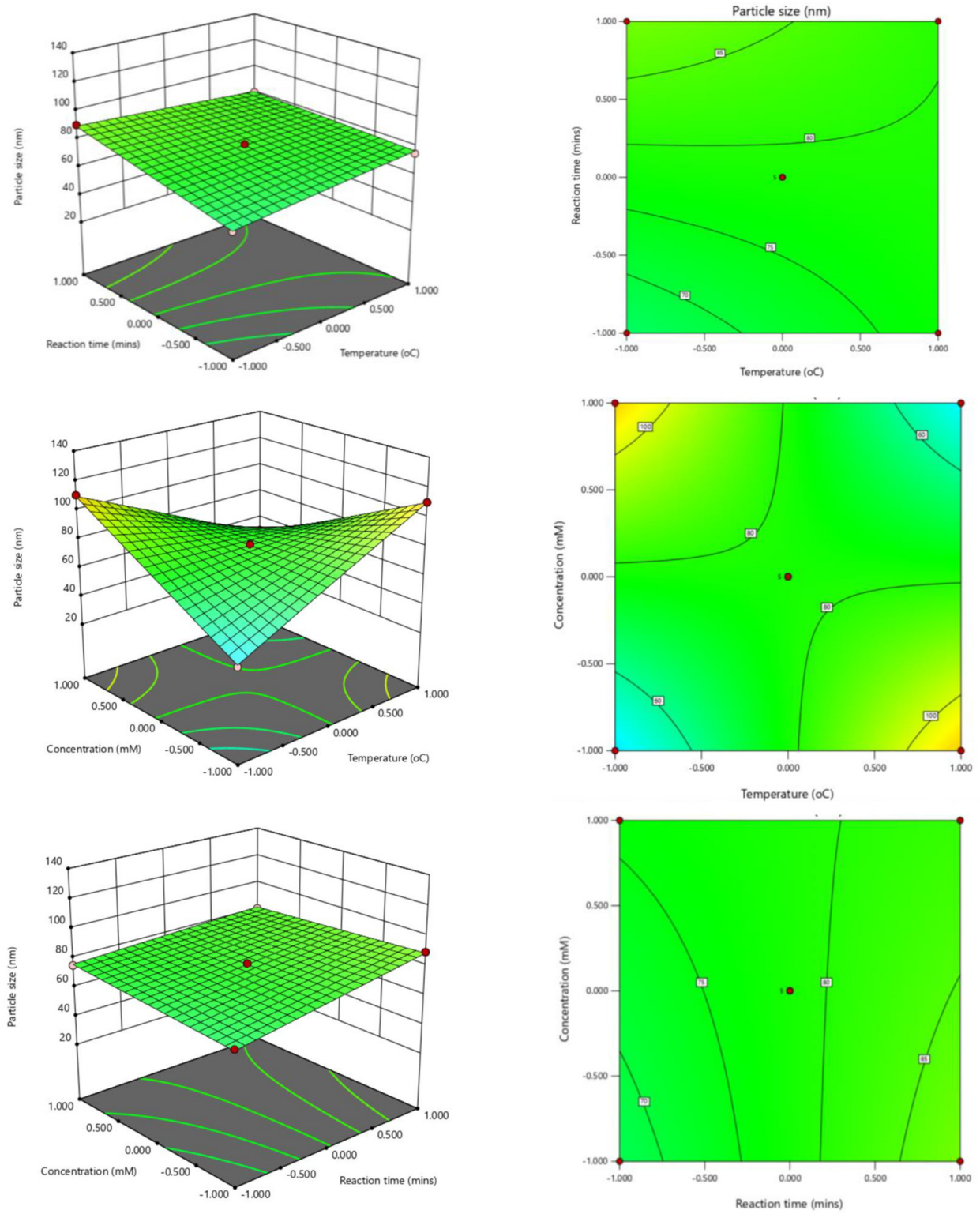


Figure 2. Response surface plot showing the effects of the interactions of various parameters on the particle size of Ag-NPs.

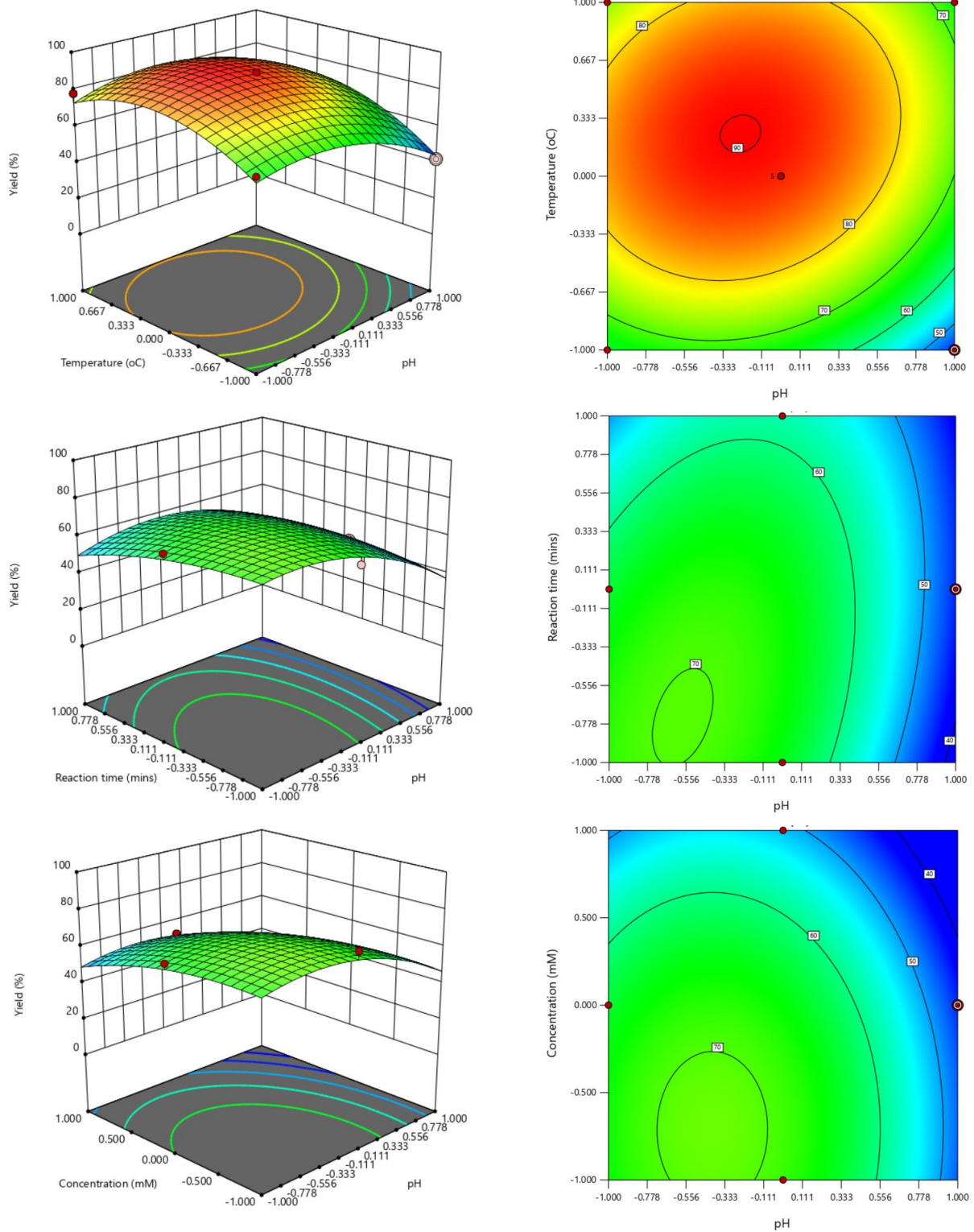


Figure 3. Cont.

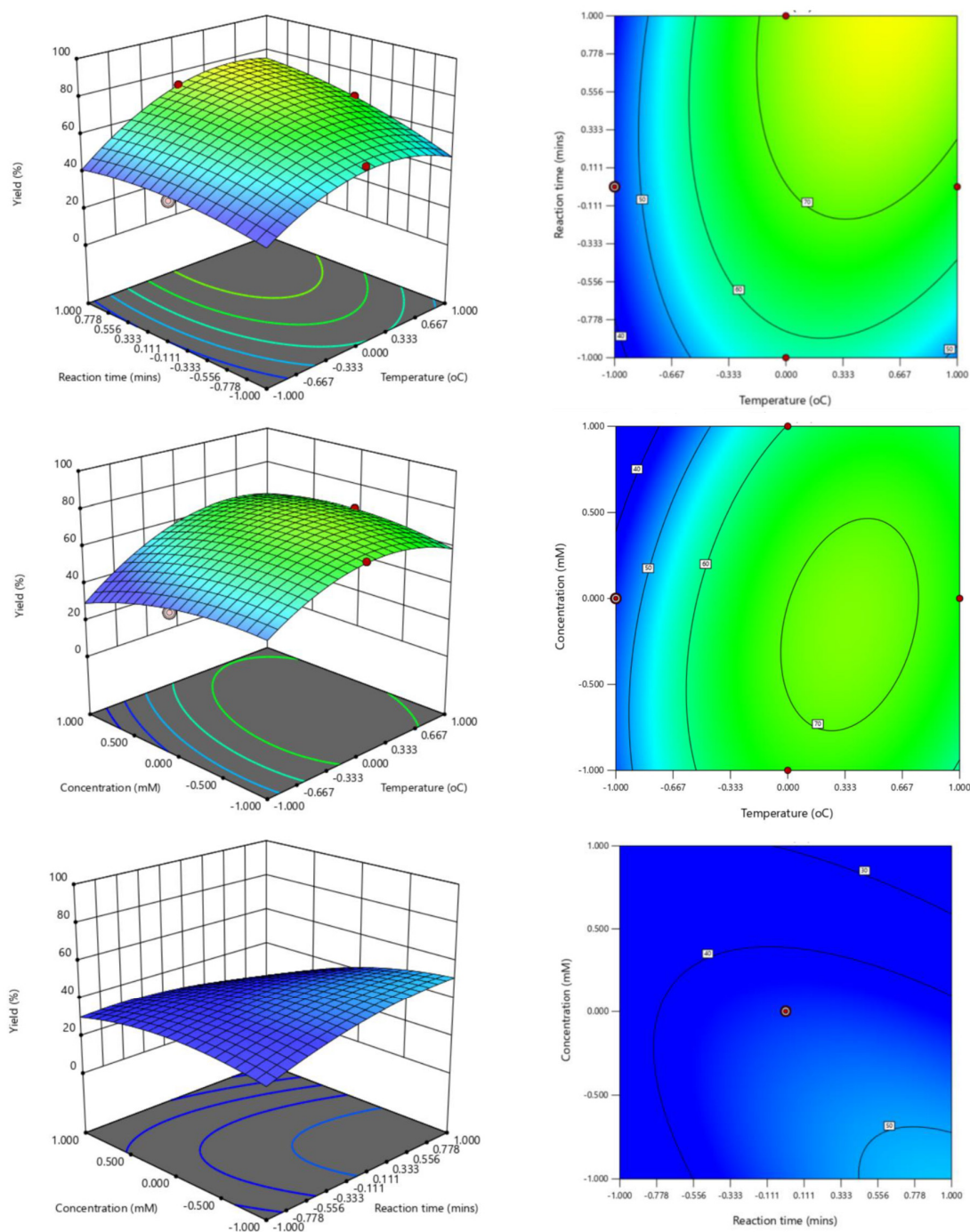


Figure 3. Response surface plot showing the effect of the interactions of various parameters on the yield of Ag-NPs.

3.3. *In Vitro* Anti-*Alternaria* Activity of Phyto-Synthesized Ag-NPs

In vitro anti-*alternaria* activity of the synthesized nanoparticles showed a concentration-dependent inhibition of the fungi mycelia (Figure 4a) with 200 ppm having the highest inhibition of 54.61% which was significantly different with propiconazole with a 100% inhibition of the mycelia at the end of 7-days of the incubation period (Figure 4b). Figure 5a,b show the mycelia of *A. alternata* mycelia treated with Ag-NPs under scanning and transmission electron microscopes, respectively. The mycelia of the fungus treated with Ag-NPs were shrunken and shriveled compared with the control fungus under scanning electron microscope (Figure 5c), while transmission electron microscope images showed a clearance

or disappearance of the cytoplasmic organelles such as mitochondria and food vacuole, and a thinner cell wall in the treated fungus compared with the control sample which maintained its organelles (Figure 5c,d). The elemental composition of the mycelia of the fungi sample treated with Ag-NPs and the control confirmed the localization of Ag-NPs within the cell of the fungus treated with the nanoparticle (Figure 5e,f).

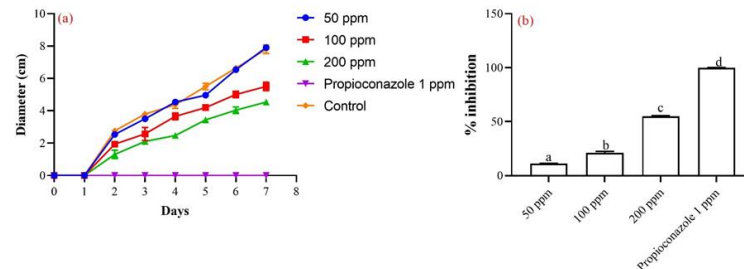


Figure 4. (a) Mycelia growth and (b) Percentage inhibition of *Alternaria alternata* mycelia treated with different concentrations of phyto-synthesized Ag-NPs. Bars with different letters of alphabets (a–d) have values that are statistically significant at $p < 0.05$.

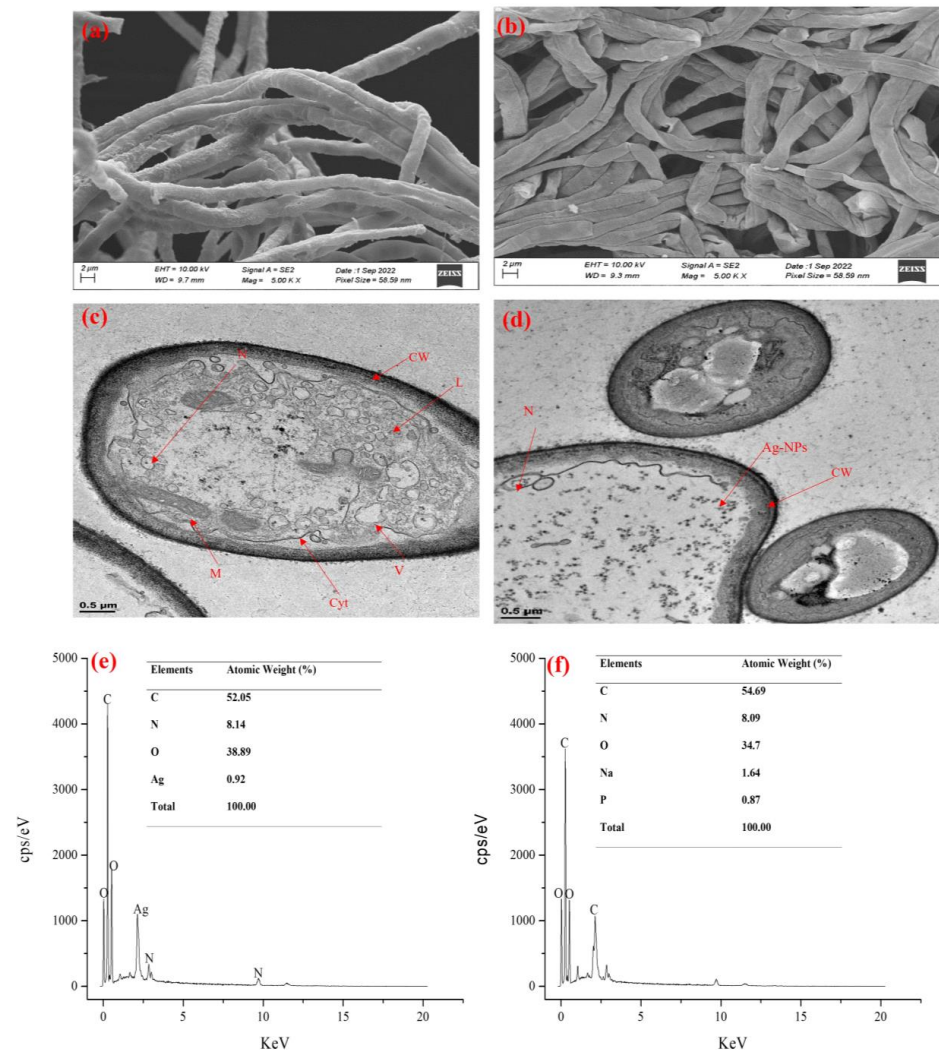


Figure 5. SEM and TEM micrograph of *Alternaria alternata* treated with 200 ppm of Ag-NPs (a,b), control (c,d), and EDX of *Alternaria alternata* mycelia treated with 200 ppm of (e) Ag-NPs and (f) control. Keys = Ag-NPs: silver nanoparticles, CW: Cell wall, FV: Food vacuole, M: Mitochondria, N: Nucleus.

3.4. Effects of Ag-NPs Treatment on Biochemical Contents and Enzyme Activity of *A. alternata*

Extracellular and intracellular polysaccharide contents of the fungi treated with 200 ppm of Ag-NPs are presented in Figure 6a. The results showed no significant difference ($p > 0.05$) in the extracellular content of the fungus treated with the nanoparticles compared to the control group, while the intracellular content showed a significant reduction ($p < 0.05$) in the polysaccharide content of the treated fungus. The chitin content of the fungus was significantly reduced ($p < 0.05$) after treatment with the nanoparticles compared to the control which was not treated (Figure 6b). Cellulase activity of the fungus treated with 200 ppm of Ag-NPs was determined and the results showed a significant reduction ($p < 0.05$) in the endo- β -1,4- and exo- β -1,4-glucanase activity of the fungus treated with Ag-NPs, propiconazole, and the control group (Figure 6c). Also, there was a significant reduction ($p < 0.05$) in the extracellular and intracellular lipase activity of the fungi treated with Ag-NPs compared to the control and propiconazole-treated group (Figure 6d) confirming the effect of the treatment in the reduction of the enzymatic activity of the fungi.

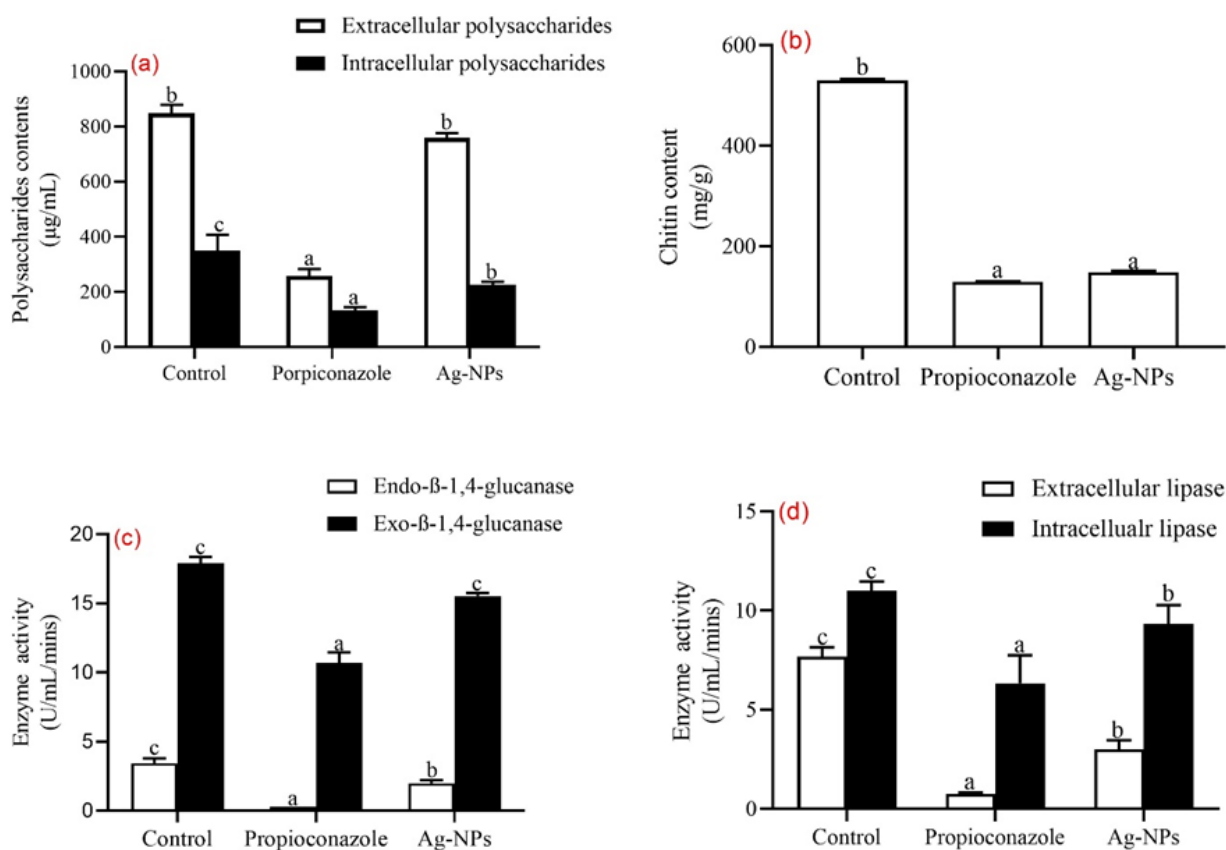


Figure 6. Effect of Ag-NP treatment on (a) polysaccharides content, (b) chitin content, (c) cellulase activity, and (d) lipase activity of *A. alternata*. Bars with different letters of alphabets (a–c) have values that are statistically significant at $p < 0.05$.

4. Discussion

In this study, optimization and characterization of phyto-synthesis Ag-NPs using Box-Behnken design and its anti-alternaria activity was carried out. The rapid increase in the applications of Ag-NPs has led to different methods of synthesis such as physical, chemical, and biological synthesis [37]. Due to their numerous advantages, the emphasis is more on the synthesis of nanomaterials from biological sources as opposed to other methods of synthesis [37,38]. The immediate reduction of Ag ions by the seed extract *A. precatiorius* was observed through a color change from light yellow to brown because of Ag-NP formation. The UV_{max} spectrum of the synthesized Ag-NPs showed a clear and

distinct peak at 409.01 nm (Figure 1a) due to its characteristic Surface Plasmon Resonance (SPR). The observed peak was within the range of UV absorbance reported by Elshafei et al. [13]. UV-visible spectroscopy is the primary confirmatory test to establish the synthesis of nanoparticles [39]. Also, the UV-visible range of Ag-NPs has been reported to be within the range of 400–430 nm, and changes in the UV absorption can be influenced by different factors such as the amount of plant extract or capping agent used in incubation time, and the concentration of AgNO₃ used for the synthesis [13,39–41]. The SEM micrograph showed face-centered cubic nanoparticles (Figure 1b) while the TEM micrograph showed that the phyto-synthesized Ag-NPs were spherical with a particle size of 23.94 ± 5.17 nm and were not in direct contact with one another (Figure 1c,d) due to the stabilization of the nanoparticles by the seed extract of *A. precatorious*, secondary metabolites such as phenols and flavonoids, which are good natural reducing agents [13]. The XRD plot revealed peaks at different θ values which were characteristics of Ag-NPs and matched the JCP2 file number, 04-0783, of Ag-NPs with a crystallite size of ~23.75 nm (Figure 1e). Further characterization using EDX analysis revealed sharp peaks at 3.2 KeV which is characteristic of Ag-NPs with 76.49% Ag, 22.73% O, and 0.78% Cu (Figure 1f). The presence of Cu and O may be attributed to impurities contained in AgNO₃ and NaOH salts used for the synthesis of the nanoparticles. The reported data is consistent with the previous report by Elshafei et al. [13] and Sahayaraj et al. [41].

The term “optimization” refers to all procedures used to regulate reaction parameters, including temperature, pH, incubation or reaction time, and concentration of silver salt, in order to produce Ag-NPs with the desired yield and particle size [42]. The synthesis of Ag-NPs was performed using 29 designed experiments according to the BBD. Different combinations of the four individual variables were used and the transformed form of experimental size was fitted to the polynomial model. The experiments were randomized, and each independent variable was placed at one of three equally spaced values (−1, 0, and +1) (Table 1) to obtain the average particle size and yield of the synthesized Ag-NPs (Table S1) [14]. From the ANOVA results (Tables 2 and 3), a significant model with a *p*-value < 0.0001 and an F-value of 492.56 and 19.80 for particle size and yield respectively were obtained. It was reported that a model with a *p*-value < 0.01 would be sufficient and adequate to explain the correlation between the factors and the corresponding response under study [43,44]. Therefore, the model from the current study adequately explained the correlation between the factors under consideration and their corresponding responses with a strong positive correlation; R² = 0.9980 and 0.9519 for both responses (particle size and yield respectively). The effect of the independent variables on the response of Ag-NP particle size and yield was determined with a quadratic polynomial model created by analysis of variance (ANOVA) in Equations (3) and (4) respectively.

$$\text{Particle size (nm)} = +78.53 - 22.78 * A + 0.7250 * B + 6.89 * C + 0.5117 * D + 32.75 * AB + 5.03 * AC - 17.84 * AD - 5.08 * BC - 31.55 * BD - 3.88 * CD - 1.23 * A^2 - 0.3302 * B^2 - 0.1028 * C^2 + 0.0697D^2 \quad (3)$$

$$\text{Yield (\%)} = +88.46 - 6.45 * A + 7.84 * B + 2.10 * C - 3.7 * D + 3.33 * AB + 5.64 * AC + 0.0725 * AD + 5.74 * BC + 4.94 * BD - 7.47 * CD - 12.13 * A^2 - 14.45 * B^2 - 4.66 * C^2 - 6.09 * D^2 \quad (4)$$

where A, B, C, and D represented the pH, temperature, reaction time, and concentration, respectively.

This model can be applied to predict the particle size and yield of Ag-NPs respectively. The developed equations also showed the main parameter influencing the particle size and yield of Ag-NPs, as shown in Table 3. Furthermore, the interactions between each of the variables and their corresponding responses were shown in the 3D and 2D plots for particle size and yield of Ag-NPs, depicting the interactions between the variables when other factors were kept constant (Figures 2 and 3). The morphology and size of nanoparticles are affected by the pH of the reaction medium which could affect the stability and macromolecule charges [45]. From this study, the majority of the nanoparticles synthesized with particle sizes < 100nm were all within the alkaline pH of 9–12 with the smallest particle size (20.36 nm) obtained at a pH of 12 (Table S1). Also, the effect of pH has

been reported to affect the yield of nanoparticles. As the pH of the medium increases from acidic to alkaline, there is more hydroxyl ion (OH⁻) present to reduce Ag⁺ to Ag⁰ [46]. This also agrees with the findings of Elshafei et al. [13] who reported that the optimum pH for the synthesis of Ag-NPs is within the alkaline pH of 10–12. A pH value below or above this range drastically affects the formation of Ag-NPs. The results of the ANOVA analysis (Tables 2 and 3) showed that the effect of pH was highly significant ($p < 0.0001$) on the particle size and yield of the nanoparticles. In a study carried out on the catalytic activity of the separated fraction of Ag-NPs biosynthesized from the flower of *Cassia auriculata* in a bid to determine the impact of pH on Ag-NP particle size, it was concluded that low pH produces large particle size nanoparticles while high pH produces nanoparticles with small particle sizes [47].

Temperature is another factor that has been reported to play a major role in the synthesis of nanoparticles. From this study, temperature had no significant difference ($p = 0.1281$) in the particle size but affected the yield of Ag-NPs ($p < 0.0001$) (Tables 2 and 3). It was reported that the reduction of Ag⁺ occurs faster at elevated temperatures with drastic changes in color which will ultimately lead to a high yield of the nanoparticles [45]. The synthesis of nanoparticles at ambient temperatures has been considered favorable because of the effects of temperature on plant secondary metabolites [48]. In this study, a temperature range of 30–60 °C is the most favorable.

Reaction time has a great impact on the stability of synthesized Ag-NPs [37]. Because of the different temperature ranges used, which in turn affect the secondary metabolites present in the plant extract, it is difficult to determine the effect of reaction time on the synthesis of Ag-NPs. In this study, a 30–120 min reaction time was used (Table 1) and it shows a significant difference ($p < 0.0001$) in the particle size of the nanoparticle (Table 2). The optimum temperature for the synthesis of Ag-NPs from this study was 60 °C. It was also reported that the effect of reaction time on the synthesis of Ag-NPs depends on the plant species used, the concentration of silver salt, the volume of extracts, temperatures, and pH which are other factors that influence reaction time of synthesis [37,49,50].

An increase in salt concentration has been reported to influence the synthesis of nanoparticles because of an increase in metal ion concentrations [37]. The effect of AgNO₃ salt concentration was statistically significant ($p = 0.0047$) on the yield of Ag-NPs and not on the particle size (Tables 2 and 3) in this study. Out of a concentration range of 1–5 mM of AgNO₃ solution that was used for the synthesis of Ag-NPs in this study, a 3 mM concentration was considered the optimum because it produced Ag-NPs with a reduced particle size. The results supported the report of Seifipour et al. [50] who documented a concentration of 0.0025 M (2.5 mM) of AgNO₃ solution as the optimum salt concentration for the synthesis of Ag-NPs. Another report set the optimum concentration of AgNO₃ salt required for the synthesis of Ag-NPs at 20, 50, and 100 mM [37].

The potential of the phyto-synthesized Ag-NPs to control *Alternaria alternata* isolated from a diseased wheat plant was evaluated in vitro. The results showed a concentration-dependent inhibition of the fungus mycelia and growth (Figure 4a,b). It has been reported that Ag-NPs have anti-spore-producing fungus activity and are effective at slowing fungal growth. Ag-NPs have been reported to induce several effects on fungi, including structural modifications in hyphae, deformations in the cell wall, and damage to the membrane. The severity of the effect depends on the concentration of the nanoparticle used [51]. From this study, treatment with 200 ppm of Ag-NPs caused changes in mycelia structure characterized by hyphal deformation, shrunkenness, and flattening compared to the control sample (Figure 5a,c) under a scanning electron microscope. The unique structure of fungi cell walls is a necessary requirement for cell pathogenicity, viability, and morphogenesis. When an antifungal compound interacts with a fungal cell, the cell wall is the first point of contact before any other cellular components. The cell wall, which is mostly made up of 1,3- and 1,6-β-glucans, chitin, and glycoproteins, helps with a variety of tasks such as cell stiffness and shape, metabolism, ion exchange, and interactions with host defense mechanisms [34]. The mechanical strength of the fungal cell wall makes it an important

structure in biotic and abiotic defense [34]. From this study, it can be observed that the cell wall of the fungus treated with Ag-NPs under transmission electron microscope became thinner with deformed cytoplasmic structure compared to the control sample (Figure 5b,d). Furthermore, the ultrastructure of the mycelia showed the absence of major cellular organelles such as mitochondria and food vacuoles, with the localization of Ag-NPs within the cytoplasm of the treated fungus. Similar results were observed when *Alternaria solani* was treated with Ag-NP [52]. One potential factor contributing to this phenomenon is the interaction between Ag-NPs and phosphorous and sulfur-containing substances present both intracellularly and extracellularly. Furthermore, it is hypothesized that Ag-NPs carrying positive charges can interact with fungal membranes that possess negative charges. This interaction can lead to the disruption of cell walls and subsequent destruction of the lipid bilayer of the membrane. Consequently, intracellular ion efflux is induced, ultimately culminating in the demise of the fungal cells [52]. To further justify the invasion of Ag-NPs into the cell of the fungus, EDX analysis of the mycelia was carried out and the results showed the localization of Ag (0.92%) within the mycelia of the fungi compared to the controlled sample which showed the absence of Ag (Figure 5e,f). Both mycelia (treated and untreated) showed almost equal proportions of C, O, and N which are the major constituent of the mycelia of fungi. These findings suggest that Ag-NPs physically interact with the cell wall of *A. alternata* to interfere with its ability to develop. As a result, the toxic effects of Ag-NPs (200 ppm), which include DNA damage, vacuolation, and organelle distortion related to nanoparticles inside the cell, can be used to explain why the growth of fungal mycelia is inhibited. After destroying the fungal plasmalemma and cytoplasmic content (DNA, protein, and lipid) and eventually causing cell death, the initial stage of fungi damage may be the absorption and internalization of nanoparticles [34,53,54].

The fungal cell wall, which is crucial for preserving cellular integrity, is wrapped in a polysaccharide-rich sheath around each fungal cell. The fungal cell wall is a prime target for antifungal treatments due to its crucial protective function and the fungi-specific enzymes that produce it [55,56]. A strong antimicrobial agent will be able to mitigate this cell wall barrier in order to exact its activity on the organism. Treatment of the fungi with 200 ppm of Ag-NPs shows a significant reduction ($p < 0.05$) in the extracellular and intracellular polysaccharides contents of the fungus and a drastic reduction in the chitin content of the fungus (Figure 6a,b). The significant reduction in the polysaccharide contents of the fungi is an indication of the antifungal activity of Ag-NPs. Chitin is an important part of fungal cell walls and the amount of chitin in fungal cell walls is proportional to the level of stress sustained by the fungi. Increased chitin content makes cell walls stiffer to withstand pressure from the environment. In response to damage to the cell wall, class IV enzymes, particularly *ScChs3* and *CaChs3* frequently produce excess chitin [57]. The disruption of chitin synthesis causes the fungal cell to become disorganized, which causes it to become distorted and osmotically unstable [58]. The decrease in the chitin content is an indication of the inhibitory activity of the nanoparticle to prevent the fungus from defending itself against the toxicity of the nanoparticle. This finding supported the literature claim about the antifungal activity of Ag-NPs. Furthermore, the effect of the nanoparticles on the enzymatic activities of the fungal showed that treatment with Ag-NPs caused a significant reduction ($p < 0.05$) in the glucanase and lipase activities of the fungal (Figure 6c,d). A variety of microorganisms, including fungi, bacteria, and archaea, produce the group of enzymes known as cellulases [59]. As cellulose is broken down by these enzymes, glucose and other molecules of fermentable sugar are produced. Endoglucanases arbitrarily cleave internal β -1,4-glucan linkages and β -glucosidases reduce disaccharides to release glucose units, exoglucanases work on the reducing and nonreducing ends of cellulose to remove cellobiose moieties [60]. This further confirms the potential of Ag-NPs as potent antifungal agents that can be used to control the spread of *A. alternata* in crops.

5. Conclusions

The synthesis of Ag-NPs from the seed extract *A. precatorious* was carried out under these optimum conditions: pH of 12 at 60 °C, 75 min reaction time, and a 3 mM concentration of AgNO₃. The nanoparticle synthesis was confirmed and characterized using UV-spectroscopy, SEM, EDS, TEM, and XRD analysis indicating that the extract can be used as a capping/reducing agent for the synthesis of Ag-NPs. The synthesized nanoparticles caused a significant inhibition of *A. alternata* mycelia at 50, 100, and 200 ppm. The effect of the nanoparticles was viewed under SEM and TEM and the results showed an alteration of the hyphal and mycelia of the fungi, while EDS analysis confirmed the localization of the nanoparticle in the cytoplasm of the fungi. The antifungal mechanism of Ag-NPs is hypothesized to be associated with the disruption of the lipid bilayer of the fungal membrane, which then leads to the efflux of intracellular ions and ultimately culminates in the death of the fungal cell. Furthermore, the accumulation of Ag-NPs within the cell wall and their interaction with DNA may have the potential to induce cellular apoptosis. These findings may provide opportunities for the potential development of effective nano bio-fungicides, serving as viable alternatives to chemical fungicides. Additionally, the utilization of enhanced and adapted porous nanoparticles might be leveraged for the administration of potent fungicides. Therefore, it is necessary to conduct comprehensive experimental trials on plants to establish the practicality of utilizing synthesized nanoparticles for the purpose of managing plant diseases.

Supplementary Materials: The following supporting information can be downloaded at: <https://www.mdpi.com/article/10.3390/cleantechnol5040068/s1>, Table S1: Actual and Predicted coded values of the experimented Box-Behnken Design for particle size and yield.

Author Contributions: Conceptualization, A.I.D., M.K. and A.K.; methodology, A.I.D., A.A.-H. and A.K.; software, A.I.D.; validation, A.A.-H., M.K. and A.K.; formal analysis, A.I.D. and A.K.; investigation, A.I.D., M.K. and A.K.; resources, M.K. and A.K.; data curation, A.I.D. and A.A.-H.; writing—original draft preparation, A.I.D.; writing—review and editing, M.K. and A.K.; visualization, A.I.D. and A.K.; supervision, M.K. and A.K.; project administration, A.K.; funding acquisition, M.K. and A.K. All authors have read and agreed to the published version of the manuscript.

Funding: This research was funded by Department of Science and Innovation (DSI); and the Technology Innovation Agency (TIA), distributed by GrainSA, grant number GB0200065 and GB0200066, the DST-NRF Centre of Excellence in Food Security (Project ID: 170202), and Tertiary Education Trust Fund (TETFund) for funding Augustine Innalegwu Daniel. The APC was funded by the University of the Western Cape.

Institutional Review Board Statement: Not applicable.

Informed Consent Statement: Not applicable.

Data Availability Statement: Data are contained within the article and Supplementary Materials.

Conflicts of Interest: The authors declare no conflict of interest. The funders had no role in the design of the study; in the collection, analyses, or interpretation of data; in the writing of the manuscript; or in the decision to publish the results.

References

1. Malandrakis, A.A.; Kavroulakis, N.; Chrysikopoulos, C.V. Zinc nanoparticles: Mode of action and efficacy against boscalid-resistant *Alternaria alternata* isolates. *Sci. Total Environ.* **2022**, *829*, 154638. [CrossRef] [PubMed]
2. Troncoso-Rojas, R.; Tiznado-Hernández, M.E. *Alternaria alternata* (black rot, black spot). In *Postharvest Decay*; Elsevier: Amsterdam, The Netherlands, 2014; pp. 147–187.
3. Wojciechowska, E.; Weinert, C.H.; Egert, B.; Trierweiler, B.; Schmidt-Heydt, M.; Horneburg, B.; Graeff-Hönninger, S.; Kulling, S.E.; Geisen, R. Chlorogenic acid, a metabolite identified by untargeted metabolome analysis in resistant tomatoes, inhibits the colonization by *Alternaria alternata* by inhibiting alternariol biosynthesis. *Eur. J. Plant Pathol.* **2014**, *139*, 735–747. [CrossRef]
4. Corkley, I.; Fraaije, B.; Hawkins, N. Fungicide resistance management: Maximizing the effective life of plant protection products. *Plant Pathol.* **2022**, *71*, 150–169. [CrossRef]

5. Malandrakis, A.A.; Apostolidou, Z.A.; Louka, D.; Markoglou, A.; Flouri, F. Biological and molecular characterization of field isolates of *Alternaria alternata* with single or double resistance to respiratory complex II and III inhibitors. *Eur. J. Plant Pathol.* **2018**, *152*, 199–211. [[CrossRef](#)]
6. Malandrakis, A.A.; Vattis, K.N.; Markoglou, A.N.; Karaoglanidis, G.S. Characterization of boscalid-resistance conferring mutations in the SdhB subunit of respiratory complex II and impact on fitness and mycotoxin production in *Penicillium expansum* laboratory strains. *Pestic. Biochem. Physiol.* **2017**, *138*, 97–103. [[CrossRef](#)] [[PubMed](#)]
7. Avenot, H.; Michailides, T. Detection of isolates of *Alternaria alternata* with multiple-resistance to fludioxonil, cyprodinil, boscalid and pyraclostrobin in *California pistachio* orchards. *Crop Prot.* **2015**, *78*, 214–221. [[CrossRef](#)]
8. Sang, H.; Lee, H.B. Molecular mechanisms of succinate dehydrogenase inhibitor resistance in phytopathogenic fungi. *Res. Plant Dis.* **2020**, *26*, 1–7.
9. Sierotzki, H.; Scalliet, G. A review of current knowledge of resistance aspects for the next-generation succinate dehydrogenase inhibitor fungicides. *Phytopathology* **2013**, *103*, 880–887. [[CrossRef](#)]
10. Malandrakis, A.A.; Kavroulakis, N.; Chrysikopoulos, C.V. Use of copper, silver and zinc nanoparticles against foliar and soil-borne plant pathogens. *Sci. Total Environ.* **2019**, *670*, 292–299. [[CrossRef](#)]
11. Huang, W.; Wang, C.; Duan, H.; Bi, Y.; Wu, D.; Du, J.; Yu, H. Synergistic antifungal effect of biosynthesized silver nanoparticles combined with fungicides. *Int. J. Agric. Biol.* **2018**, *20*, 1225–1229.
12. Malandrakis, A.A.; Kavroulakis, N.; Avramidou, M.; Papadopoulou, K.K.; Tsaniklidis, G.; Chrysikopoulos, C.V. Metal nanoparticles: Phytotoxicity on tomato and effect on symbiosis with the *Fusarium solani* FsK strain. *Sci. Total Environ.* **2021**, *787*, 147606. [[CrossRef](#)] [[PubMed](#)]
13. Elshafei, A.M.; Othman, A.M.; Elsayed, M.A.; Al-Balakocy, N.G.; Hassan, M.M. Green synthesis of silver nanoparticles using *Aspergillus oryzae* NRRL447 exogenous proteins: Optimization via central composite design, characterization and biological applications. *Environ. Nanotechnol. Monit. Manag.* **2021**, *16*, 100553. [[CrossRef](#)]
14. Barabadi, H.; Honary, S.; Ebrahimi, P.; Alizadeh, A.; Naghibi, F.; Saravanan, M. Optimization of myco-synthesized silver nanoparticles by response surface methodology employing Box-Behnken design. *Inorg. Nano-Met. Chem.* **2019**, *49*, 33–43. [[CrossRef](#)]
15. Castro-Mayorga, J.L.; Freitas, F.; Reis, M.; Prieto, M.A.; Lagaron, J. Biosynthesis of silver nanoparticles and polyhydroxybutyrate nanocomposites of interest in antimicrobial applications. *Int. J. Biol. Macromol.* **2018**, *108*, 426–435. [[CrossRef](#)] [[PubMed](#)]
16. Saravanan, M.; Gopinath, V.; Chaurasia, M.K.; Syed, A.; Ameen, F.; Purushothaman, N. Green synthesis of anisotropic zinc oxide nanoparticles with antibacterial and cytofriendly properties. *Microb. Pathog.* **2018**, *115*, 57–63. [[CrossRef](#)] [[PubMed](#)]
17. Kumar, V.; Singh, S.; Srivastava, B.; Bhadouria, R.; Singh, R. Green synthesis of silver nanoparticles using leaf extract of *Holoptelea integrifolia* and preliminary investigation of its antioxidant, anti-inflammatory, antidiabetic and antibacterial activities. *J. Environ. Chem. Eng.* **2019**, *7*, 103094. [[CrossRef](#)]
18. Vasantharaj, S.; Sathiyavimal, S.; Saravanan, M.; Senthilkumar, P.; Gnanasekaran, K.; Shanmugavel, M.; Manikandan, E.; Pugazhendhi, A. Synthesis of ecofriendly copper oxide nanoparticles for fabrication over textile fabrics: Characterization of antibacterial activity and dye degradation potential. *J. Photochem. Photobiol. B Biol.* **2019**, *191*, 143–149. [[CrossRef](#)]
19. Nasrollahzadeh, M.; Mahmoudi-Gom Yek, S.; Motahharifar, N.; Ghafari Gorab, M. Recent developments in the plant-mediated green synthesis of Ag-based nanoparticles for environmental and catalytic applications. *Chem. Rec.* **2019**, *19*, 2436–2479. [[CrossRef](#)]
20. Gour, A.; Jain, N.K. Advances in green synthesis of nanoparticles. *Artif. Cells Nanomed. Biotechnol.* **2019**, *47*, 844–851. [[CrossRef](#)]
21. Akintelu, S.A.; Folorunso, A.S.; Folorunso, F.A.; Oyebamiji, A.K. Green synthesis of copper oxide nanoparticles for biomedical application and environmental remediation. *Heliyon* **2020**, *6*, e04508. [[CrossRef](#)]
22. Huang, L.; Luo, F.; Chen, Z.; Megharaj, M.; Naidu, R. Green synthesized conditions impacting on the reactivity of Fe NPs for the degradation of malachite green. *Spectrochim. Acta Part A Mol. Biomol. Spectrosc.* **2015**, *137*, 154–159. [[CrossRef](#)] [[PubMed](#)]
23. Jacob, P.J.; Masarudin, M.J.; Hussein, M.Z.; Rahim, R.A. Optimization of process parameters influencing the sustainable construction of iron oxide nanoparticles by a novel tropical wetlands *Streptomyces* spp. *J. Clean. Prod.* **2019**, *232*, 193–202. [[CrossRef](#)]
24. Chowdhury, S.; Yusof, F.; Faruck, M.O.; Sulaiman, N. Process optimization of silver nanoparticle synthesis using response surface methodology. *Procedia Eng.* **2016**, *148*, 992–999. [[CrossRef](#)]
25. Castaldi, S.; Zorrilla, J.G.; Petrillo, C.; Russo, M.T.; Ambrosino, P.; Masi, M.; Cimmino, A.; Istatico, R. *Alternaria alternata* isolated from infected pears (*Pyrus communis*) in Italy produces non-host toxins and hydrolytic enzymes as infection mechanisms and exhibits competitive exclusion against *Botrytis cinerea* in co-infected host fruits. *J. Fungi* **2023**, *9*, 326. [[CrossRef](#)] [[PubMed](#)]
26. Chi, N.T.L.; Narayanan, M.; Chinnathambi, A.; Govindasamy, C.; Subramani, B.; Brindhadevi, K.; Pimpimon, T.; Pikulkaew, S. Fabrication, characterization, anti-inflammatory, and anti-diabetic activity of silver nanoparticles synthesized from *Azadirachta indica* kernel aqueous extract. *Environ. Res.* **2022**, *208*, 112684.
27. Bashir, M.R.; Atiq, M.; Sajid, M.; Mohsan, M.; Abbas, W.; Alam, M.W.; Bashair, M. Antifungal exploitation of fungicides against *Fusarium oxysporum* f. sp. *capsici* causing Fusarium wilt of chilli pepper in Pakistan. *Environ. Sci. Pollut. Res.* **2018**, *25*, 6797–6801. [[CrossRef](#)]
28. Philippe, S.; Souaïbou, F.; Guy, A.; Sébastien, D.T.; Boniface, Y.; Paulin, A.; Issaka, Y.; Dominique, S. Chemical Composition and Antifungal activity of Essential oil of Fresh leaves of *Ocimum gratissimum* from Benin against six Mycotoxigenic Fungi isolated from traditional cheese wagashi. *Int. Res. J. Biol. Sci.* **2012**, *1*, 22–27.

29. Li, J.; Fu, S.; Fan, G.; Li, D.; Yang, S.; Peng, L.; Pan, S. Active compound identification by screening 33 essential oil monomers against *Botryosphaeria dothidea* from postharvest kiwifruit and its potential action mode. *Pestic. Biochem. Physiol.* **2021**, *179*, 104957. [[CrossRef](#)]
30. Raliya, R.; Tarafdar, J.C.; Biswas, P. Enhancing the mobilization of native phosphorus in the mung bean rhizosphere using ZnO nanoparticles synthesized by soil fungi. *J. Agric. Food Chem.* **2016**, *64*, 3111–3118. [[CrossRef](#)]
31. Ospina Álvarez, S.P.; Ramírez Cadavid, D.A.; Escobar Sierra, D.M.; Ossa Orozco, C.P.; Rojas Vahos, D.F.; Zapata Ocampo, P.; Atehortúa, L. Comparison of extraction methods of chitin from *Ganoderma lucidum* mushroom obtained in submerged culture. *Biomed Res. Int.* **2014**, *2014*, 169071. [[CrossRef](#)]
32. Sinegani, A.A.S.; Emtiazi, G. The relative effects of some elements on the DNS method in cellulase assay. *J. Appl. Sci. Environ. Manag.* **2006**, *10*, 93–96. [[CrossRef](#)]
33. Ang, S.; Shaza, E.; Adibah, Y.; Suraini, A.; Madihah, M. Production of cellulases and xylanase by *Aspergillus fumigatus* SK1 using untreated oil palm trunk through solid state fermentation. *Process Biochem.* **2013**, *48*, 1293–1302. [[CrossRef](#)]
34. Dhiman, S.; Varma, A.; Prasad, R.; Goel, A. Mechanistic Insight of the Antifungal Potential of Green Synthesized Zinc Oxide Nanoparticles against *Alternaria brassicae*. *J. Nanomater.* **2022**, *2022*, 7138843. [[CrossRef](#)]
35. Iftikhar, T.; Abdullah, R.; Iqtedar, M.; Kaleem, A.; Aftab, M.; Niaz, M.; Sidra, B.T.; Majeed, H. Production of lipases by *Alternaria* sp.(mbl 2810) through optimization of environmental conditions using submerged fermentation technique. *Int. J. Biosci.* **2015**, *6655*, 178–186.
36. Selvam, K.; Vishnupriya, B.; Bose, V.S.C. Screening and quantification of marine actinomycetes producing industrial enzymes amylase, cellulase and lipase from south coast of India. *Int. J. Pharma Bio Sci.* **2011**, *2*, 1481–1487.
37. Akintelu, S.A.; Olugbeko, S.C.; Folorunso, A.S.; Oyebamiji, A.K.; Folorunso, F.A. Potentials of phytosynthesized silver nanoparticles in biomedical fields: A review. *Int. Nano Lett.* **2021**, *11*, 273–293. [[CrossRef](#)]
38. Folorunso, A.; Akintelu, S.; Oyebamiji, A.K.; Ajayi, S.; Abiola, B.; Abdusalam, I.; Morakinyo, A. Biosynthesis, characterization and antimicrobial activity of gold nanoparticles from leaf extracts of *Annona muricata*. *J. Nanostruct. Chem.* **2019**, *9*, 111–117. [[CrossRef](#)]
39. Khan, M.N.; Khan, T.A.; Khan, Z.; Al-Thabaiti, S.A. Green synthesis of biogenic silver nanomaterials using *Raphanus sativus* extract, effects of stabilizers on the morphology, and their antimicrobial activities. *Bioprocess Biosyst. Eng.* **2015**, *38*, 2397–2416. [[CrossRef](#)]
40. Ahmed, S.; Ahmad, M.; Swami, B.L.; Ikram, S. A review on plants extract mediated synthesis of silver nanoparticles for antimicrobial applications: A green expertise. *J. Adv. Res.* **2016**, *7*, 17–28. [[CrossRef](#)]
41. Sahayaraj, K.; Balasubramanyam, G.; Chavali, M. Green synthesis of silver nanoparticles using dry leaf aqueous extract of *Pongamia glabra* Vent (Fab.), Characterization and phytofungicidal activity. *Environ. Nanotechnol. Monit. Manag.* **2020**, *14*, 100349. [[CrossRef](#)]
42. Mittal, A.K.; Chisti, Y.; Banerjee, U.C. Synthesis of metallic nanoparticles using plant extracts. *Biotechnol. Adv.* **2013**, *31*, 346–356. [[CrossRef](#)] [[PubMed](#)]
43. Siti, R.M.; Khairunisak, A.R.; Aziz, A.A.; Noordin, R. Green synthesis of 10 nm gold nanoparticles via seeded-growth method and its conjugation properties on lateral flow immunoassay. *Adv. Mater. Res.* **2013**, *686*, 8–12. [[CrossRef](#)]
44. Usman, A.I.; Aziz, A.A.; Sodipo, B.K. Application of central composite design for optimization of biosynthesized gold nanoparticles via sonochemical method. *SN Appl. Sci.* **2019**, *1*, 403. [[CrossRef](#)]
45. Verma, A.; Mehata, M.S. Controllable synthesis of silver nanoparticles using Neem leaves and their antimicrobial activity. *J. Radiat. Res. Appl. Sci.* **2016**, *9*, 109–115. [[CrossRef](#)]
46. Traiwatcharanon, P.; Timsorn, K.; Wongchoosuk, C. Effect of pH on the green synthesis of silver nanoparticles through reduction with pistiastratiotes I. extract. *Adv. Mater. Res.* **2016**, *1131*, 223–226. [[CrossRef](#)]
47. Muthu, K.; Priya, S. Green synthesis, characterization and catalytic activity of silver nanoparticles using *Cassia auriculata* flower extract separated fraction. *Spectrochim. Acta Part A Mol. Biomol. Spectrosc.* **2017**, *179*, 66–72. [[CrossRef](#)]
48. Fanoro, O.T.; Parani, S.; Maluleke, R.; Lebepe, T.C.; Varghese, R.J.; Mgedle, N.; Mavumengwana, V.; Oluwafemi, O.S. Biosynthesis of smaller-sized platinum nanoparticles using the leaf extract of *Combretum erythrophyllum* and its antibacterial activities. *Antibiotics* **2021**, *10*, 1275. [[CrossRef](#)]
49. Khalil, M.M.; Ismail, E.H.; El-Baghdady, K.Z.; Mohamed, D. Green synthesis of silver nanoparticles using olive leaf extract and its antibacterial activity. *Arab. J. Chem.* **2014**, *7*, 1131–1139. [[CrossRef](#)]
50. Seifipour, R.; Nozari, M.; Pishkar, L. Green synthesis of silver nanoparticles using *Tragopogon collinus* leaf extract and study of their antibacterial effects. *J. Inorg. Organomet. Polym. Mater.* **2020**, *30*, 2926–2936. [[CrossRef](#)]
51. Villamizar-Gallardo, R.; Cruz, J.F.O.; Ortíz-Rodríguez, O.O. Fungicidal effect of silver nanoparticles on toxigenic fungi in cocoa. *Pesqui. Agropecuária Bras.* **2016**, *51*, 1929–1936. [[CrossRef](#)]
52. Abdel-Hafez, S.I.; Nafady, N.A.; Abdel-Rahim, I.R.; Shaltout, A.M.; Daròs, J.-A.; Mohamed, M.A. Assessment of protein silver nanoparticles toxicity against pathogenic *Alternaria solani*. *3 Biotech* **2016**, *6*, 199. [[CrossRef](#)]
53. Cai, L.; Chen, J.; Liu, Z.; Wang, H.; Yang, H.; Ding, W. Magnesium oxide nanoparticles: Effective agricultural antibacterial agent against *Ralstonia solanacearum*. *Front. Microbiol.* **2018**, *9*, 790. [[CrossRef](#)] [[PubMed](#)]
54. Chen, J.; Wu, L.; Lu, M.; Lu, S.; Li, Z.; Ding, W. Comparative study on the fungicidal activity of metallic MgO nanoparticles and macroscale MgO against soilborne fungal phytopathogens. *Front. Microbiol.* **2020**, *11*, 365. [[CrossRef](#)] [[PubMed](#)]

55. Munro, C.A. Chitin and glucan, the yin and yang of the fungal cell wall, implications for antifungal drug discovery and therapy. In *Advances in Applied Microbiology*; Elsevier: Amsterdam, The Netherlands, 2013; Volume 83, pp. 145–172.
56. Gow, N.A.; Latge, J.-P.; Munro, C.A. The fungal cell wall: Structure, biosynthesis, and function. *Microbiol. Spectr.* **2017**, *5*, 178–186. [[CrossRef](#)] [[PubMed](#)]
57. Alanazi, H.; Semlali, A.; Perraud, L.; Chmielewski, W.; Zakrzewski, A.; Rouabhia, M. Cigarette smoke-exposed *Candida albicans* increased chitin production and modulated human fibroblast cell responses. *BioMed Res. Int.* **2014**, *2014*, 963156. [[CrossRef](#)]
58. Lenardon, M.D.; Munro, C.A.; Gow, N.A. Chitin synthesis and fungal pathogenesis. *Curr. Opin. Microbiol.* **2010**, *13*, 416–423. [[CrossRef](#)]
59. Meneses, C.; Silva, B.; Medeiros, B.; Serrato, R.; Johnston-Monje, D. A metagenomic advance for the cloning and characterization of a cellulase from red rice crop residues. *Molecules* **2016**, *21*, 831. [[CrossRef](#)]
60. Sharma, A.; Tewari, R.; Rana, S.S.; Soni, R.; Soni, S.K. Cellulases: Classification, methods of determination and industrial applications. *Appl. Biochem. Biotechnol.* **2016**, *179*, 1346–1380. [[CrossRef](#)]

Disclaimer/Publisher’s Note: The statements, opinions and data contained in all publications are solely those of the individual author(s) and contributor(s) and not of MDPI and/or the editor(s). MDPI and/or the editor(s) disclaim responsibility for any injury to people or property resulting from any ideas, methods, instructions or products referred to in the content.